2004

Numerical Analysis of a Miniature-Scale Refrigeration System (MSRS) for Electronics Cooling

Suwat Trutassanawin
Purdue University

Eckhard A. Groll
Purdue University

NUMERICAL ANALYSIS OF A MINIATURE-SCALE REFRIGERATION SYSTEM (MSRS) FOR ELECTRONICS COOLING

Suwat Trutassanawin[1] and Eckhard A. Groll

Purdue University
School of Mechanical Engineering
Ray W. Herrick Laboratories
West Lafayette, Indiana, USA

[1] Corresponding Author: (765) 495-7515; e-mail: strutas1@purdue.edu

ABSTRACT

This paper presents the numerical analysis of a Miniature-Scale Refrigeration System (MSRS) for electronics cooling. The system consists of a simulated electronic chip attached to a microchannel cold plate evaporator, a compressor, a microchannel condenser, and an expansion device. The system uses R-134a as the refrigerant. A copper block heater is designed to simulate the heat generation of an electronic chip by using two cartridge heaters of 200 W each. The heat from the simulated CPU is transferred to the cold plate evaporator via a copper heat spreader. The heat spreader is employed to provide uniform heat dissipation from the copper block to the evaporator. In order to analyze the system performance and determine the operating conditions, a numerical simulation of the MSRS was conducted. In addition, the "Fluent"-software was employed to analyze the heat spreader. Experimental results that were obtained using a bread board MSRS were used to validate the model results.

1. INTRODUCTION

The advance of the computer technology has lead to higher processor speeds, smaller sizes, and increased power consumption. Thus, the heat dissipation from the chip becomes a critical issue in the design of high performance semiconductor processors. The conventional air cooling methods using heat sinks are expected to not be able to maintain acceptable chip core temperatures in the near future. Therefore, alternative cooling approaches, such as heat pipes, thermoelectric cooling, liquid cooling, spray cooling, jet impingement cooling, and refrigeration cooling, are currently being investigated to accommodate the envisioned high heat dissipation applications. The study presented here focuses on refrigeration cooling techniques. The advantages of the refrigeration cooling technique are: (1) to maintain a low junction temperature and at the same time dissipate high heat fluxes; (2) to increase the device speed due to a lower operating temperature; and (3) to increase the device reliability and life cycle time because of a lower and constant operating temperature. The disadvantages of the refrigeration cooling technique are: (4) an increased complexity and cost; (5) the need for additional space to fit the components of the refrigeration system; and (6) a decrease of the system reliability as a result of an additional moving component, i.e., the compressor.

2. MINIATURE-SCALE REFRIGERATION SYSTEMS (MSRS) FOR ELECTRONICS COOLING

A schematic diagram of a Miniature-Scale Refrigeration System for electronics cooling is illustrated in Figure 1. The MSRS is composed of six main components: a cold plate microchannel evaporator, a compressor, a microchannel condenser, two expansion devices in parallel (a needle valve and a capillary tube), a heat spreader, as well as a heat source or heater block, which simulates the CPU. Based on the components indicated in Figure 1, a bread board MSRS was designed and constructed using a commercially available small-scale hermetic rotary compressor. The R-134a compressor is driven by a DC motor and has a cooling capacity of 75 to 140 W, a COP of 1.13 to 1.35, and a maximum power consumption of 103 W at typical hotel mini-bar refrigerator operating conditions. The heat source consists of a copper block with dimension of $19.05 \times 19.05 \times 19.05$ mm^3. Two cartridge heaters with a maximum heat dissipation power of 400 W are inserted into the base block that is below the copper

block. The base block has dimensions of $45\times32\times13$ mm^3. A variable AC transformer is used to adjust the power input to the heaters. A heat spreader is employed in order to dissipate the heat from the heat source to the heat sink. The heat spreader is made of copper with the dimensions of $50.8\times50.8\times2.5$ mm^3. A thermal conductive paste was applied between the copper block-heat spreader mating surfaces and the heat spreader-heat sink mating surfaces to reduce the thermal resistance. The thermal conductive paste has a thermal resistance of less than 0.005 °C-in^2/W for a 0.001 inch layer. The evaporator is a microchannel heat exchanger consisting of 41 rectangular channels. Each channel has a cross section area of 0.8×2.3 mm^2. The microchannel condenser has a heat dissipation capacity of 225 W and dimensions of $45\times180\times25$ mm^3. The expansion devices are composed of a capillary tube with 0.081" OD and 0.031" ID, and a hand operated needle valve. The system was charged with 100 g of R-134a. A photograph of the entire bread board MSRS is shown in Figure 2.

The target operating conditions of the MSRS are as follows: cooling capacity of 200 W; evaporating temperature range from 10 to 20°C; superheat of the refrigerant at the compressor inlet in the range of 3 to 8 °C; condensing temperature in the range of 40 to 60 °C; subcooling temperature of the refrigerant at the condenser outlet in the range of 3 to 10 °C; and ambient air temperature in the range of 30 to 50 °C.
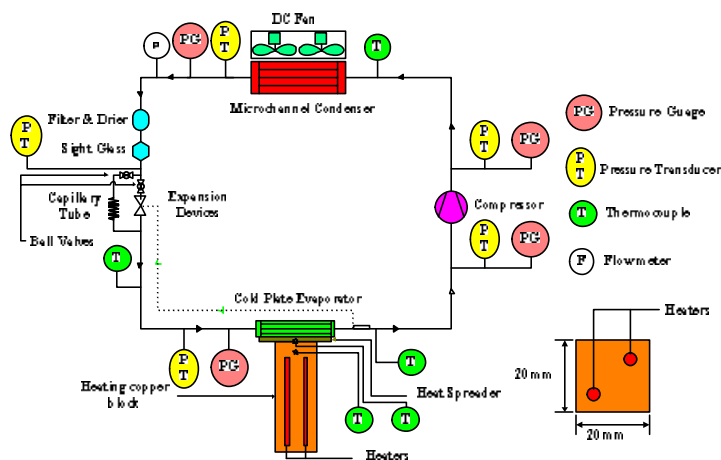

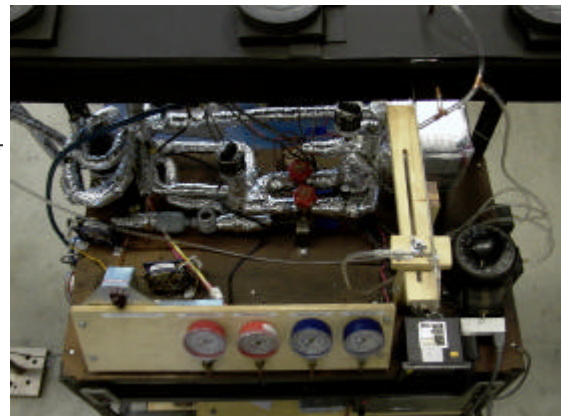Figure 1: Schematic of bread board MSRS.

Figure 2: Photograph of bread board MSRS.

3. REFRIGERATION SYSTEM MODEL

A refrigeration system simulation model was written in MATLAB. The model is divided into four parts: an evaporator model, a compressor model, a condenser model, an expansion device model. The main assumptions of the system model are negligible pressure drop in the evaporator and condenser, as well as negligible heat loss from the connecting pipes. The system model begins its calculations at the inlet to the compressor with three inputs: suction pressure, discharge pressure, and superheat temperature. The outputs of compressors model are refrigerant mass flow rate, compressor power input, and compressor outlet temperature. In the condenser model, the inlet conditions are assumed equal to the outlet of the compressor. To simplify the condenser model, a lump capacitance method was employed and the total heat rejection of the condenser was set equal to the sum of the cooling capacity of the evaporator and the power consumption of the compressor subtracting the heat loss of the compressor. The condenser outlet pressure and a guess outlet temperature of the condenser are the inputs to the expansion device model. The expansion process is assumed isenthalpic and the outlet pressure equals the compressor inlet pressure. The refrigerant quality is the output of the expansion device model. The evaporator model is divided into small segments with known inlet quality and constant pressure. The outlet state of each segment is calculated by assuming a constant heat flux to all segments. Until the segment outlet quality reaches a state of saturated vapor, a homogeneous two-phase analysis is used on each segment. Afterwards, a single phase analysis is employed. The analysis marches through the evaporator until the total length of all segments is equal to the evaporator length. The outputs of the evaporator model are local and average refrigerant heat transfer coefficients, as well as the evaporator outlet temperature. In the next step, the condenser outlet temperature is determined from the condenser model and is compared to the guess expansion device inlet temperature. If both values are not equal, then the condenser outlet

temperature is updated. The calculations are repeated until both values are equal. A flow chart of the system model is presented in Figure 3. After system convergence is achieved, the coefficient of performance (COP) and all other operating conditions are calculated. The properties of the refrigerant R-134a are calculated using the Reference Fluid Thermodynamic and Transport Properties software, REFPROP 7.0, by NIST.

3.1 Compressor model

The following assumptions are made within the compressor model: neglecting changes in kinetic and potential energy, the compressor operates at steady-state condition, and pressure losses in the suction and discharge lines are negligible. A hermetic compressor modeling approach is employed with compressor speed, swept volume, compressor inlet and outlet pressures, as well as superheat temperature as input parameters. The volumetric, isentropic, and mechanical compressor efficiencies are assumed equal to 67, 80, and 45 %, respectively. The motor efficiency is 80 % and the compressor heat loss factor is 10%.

The refrigerant mass flow rate is computed from known volumetric efficiency, compressor speed, and swept volume by the following equation:

$$h_{vol} = \frac{\dot{m}_{actual}}{\dot{m}_{theoritical}} = \frac{\dot{m}_{actual}}{N(V_{swept} / v_{in})} \tag{1}$$

The overall compressor efficiency is the product of the isentropic, mechanical, and motor efficiencies:

$$h_o = h_{isen} h_{mech} h_{motor} \tag{2}$$

The isentropic efficiency is the ratio of isentropic compression work to the actual compression work:

$$h_{isen} = \frac{\dot{W}_{isen}}{\dot{W}_{refrig}} = \frac{h_{dis,isen} - h_{suct}}{h_{dis} - h_{suct}} \tag{3}$$

The mechanical efficiency is related to the actual refrigerant compression work and the shaft work as follows:

$$h_{mech} = \frac{\dot{W}_{refrig}}{\dot{W}_{shaft}} \tag{4}$$

The total compressor power input is:

$$\dot{W}_{comp,e} = \frac{\dot{m}(h_{isen} - h_{suct})}{h_o} \tag{5}$$

The heat loss from the compressor shell is determined by equation (6):

$$\dot{Q}_{loss,shell} = f_Q(1 - h_{mech} h_{motor})\dot{W}_{comp,e} \tag{6}$$

In addition, heat transfer occurs from the discharge line back to suction refrigerant. The heat transfer is calculated by:

$$\dot{Q}_{dis\_to\_suct} = (1 - f_Q)(1 - h_{mech})\dot{W}_{comp,e} \tag{7}$$

Thus, the suction, discharge, and outlet enthalpies of the refrigerant are computed as follows:

$$h_{suct} = h_{inlet} + \frac{\dot{Q}_{dis\_to\_suct}}{\dot{m}} \tag{8}$$

$$h_{dis} = h_{suct} + \frac{\dot{W}_{comp,e} - \dot{Q}_{loss,shell}}{\dot{m}} \tag{9}$$

$$h_{outlet} = h_{dis} - \frac{\dot{Q}_{dis\_to\_suct}}{\dot{m}} \tag{10}$$

The outputs of the compressor model are the refrigerant mass flow rate, compressor outlet temperature, compressor heat loss, and compressor power input.

3.2 Condenser model

The condenser model is used by assuming lump capacitance method and neglecting pressure drop in the condenser. The total heat rejection rate equals the sum of the cooling capacity of evaporator and the compression power of refrigerant.

$$\dot{Q}_{cond} = \dot{Q}_{load} + \dot{W}_{comp} \tag{11}$$

The condenser outlet enthalpy is obtained by:

$$h_{cond,o} = h_{cond,i} - \frac{\dot{Q}_{cond}}{\dot{m}} \tag{12}$$

3.3 Expansion device model

The expansion model requires the refrigerant inlet and outlet pressures as well as an estimated expansion inlet enthalpy or temperature. An isenthalpic (constant enthalpy) process is assumed for the expansion device:

$$h_{exp,o} = h_{exp,i} \tag{13}$$

The outlet quality of the refrigerant is computed by:

$$x = \frac{h_{exp,o} - h_f}{h_{fg}} \tag{14}$$

The outlet states of expansion device are assumed to be the inlet states of the evaporator model.

3.4 Evaporator model

The following assumptions are made within the evaporator model: neglecting changes in kinetic and potential energy, steady-state operating condition, pressure drop in the cold plate is negligible, and there is no heat loss to the surroundings, i.e., the entire heat dissipated by the CPU is transferred to the cold plate evaporator. The evaporator model is divided into two regions: two-phase region and single phase or superheat region.

Two-phase region:

The two-phase heat transfer coefficient is calculated using the Kandlikar (1999) correlations [2]:

$$h_{TPh} = \text{larger of} \begin{cases} h_{TPh,NBD} \\ h_{TPh,CBD} \end{cases} \tag{15}$$

Where $h_{TP,NBD}$ and $h_{TP,CBD}$ are the two-phase heat transfer coefficients in the nucleate boiling dominant and convective boiling dominant regions, as expressed by the following equations:

$$h_{TPh,NBD} = \left(0.6683 Co^{-0.2} Fr_{lo} + 1058.0 Bo^{0.7} F_{fl}\right)(1-x)^{0.8} h_{lo} \tag{16}$$

$$h_{TPh,CBD} = \left(1.136 Co^{-0.9} Fr_{lo} + 667.2 Bo^{0.7} F_{fl}\right)(1-x)^{0.8} h_{lo} \tag{17}$$

Where, the convection number (Co) and boiling number (Bo) are defined as:

$$Co = \left(\frac{r_f}{r_g}\right)^{0.5} \left[\frac{(1-x)}{x}\right]^{0.8} \qquad\qquad Bo = \frac{q''}{Gh_{fg}} \tag{18}$$

The fluid-surface parameter for R-134a is $F_{fl} = 1.63$.

The Froude number for the whole flow as liquid, Fr_{lo}, is a parameter for the stratified flow region. For the given application, the Froude number was set equal to 1, since there is no stratified flow in microchannel heat exchangers.

The single phase heat transfer coefficient the whole flow as liquid is computed using the Gnielinski correlation [2]:

For $10^4 \leq \mathrm{Re}_{lo} \leq 5 \times 10^6$;

For $2300 \leq \mathrm{Re}_{lo} \leq 10^4$;

$$Nu_{lo} = \frac{\mathrm{Re}_{lo}\, \mathrm{Pr}_l \left(f/2 \right)}{1 + 12.7 \left(\mathrm{Pr}_l^{2/3} - 1 \right) \left(f/2 \right)^{0.5}}$$

$$Nu_{lo} = \frac{\left(\mathrm{Re}_{lo} - 1000 \right) \mathrm{Pr}_l \left(f/2 \right)}{1 + 12.7 \left(\mathrm{Pr}_l^{2/3} - 1 \right) \left(f/2 \right)^{0.5}}$$

and for $\mathrm{Re}_{lo} \leq 2300$

$$Nu_{lo} = 4.36 \tag{19}$$

Where the friction factor is calculated by,

$$f = \left[1.58 \ln \left(\mathrm{Re}_{lo} \right) - 3.28 \right]^{-2} \tag{20}$$

Single phase or superheated vapor region:

The single phase heat transfer coefficient of the superheated vapor is obtained from Gnielinski correlation [3]:

For $2300 \leq \mathrm{Re}_g \leq 5 \times 10^6$ and $0.5 \leq \mathrm{Pr}_g \leq 2000$;

$$Nu_{lo} = \frac{\left(f/8 \right) \left(\mathrm{Re}_g - 1000 \right) \mathrm{Pr}_g}{1 + 12.7 \left(f/8 \right)^{0.5} \left(\mathrm{Pr}_g^{2/3} - 1 \right)} \tag{21}$$

and for $\mathrm{Re}_{lo} \leq 2300$

$$Nu_{lo} = 4.36 \tag{22}$$

Where the friction factor is given by,

$$f = \left[0.790 \ln \left(\mathrm{Re}_g \right) - 1.64 \right]^{-2} \tag{23}$$

The average heat transfer for the whole evaporator is calculated by:

$$\overline{h}_L = \frac{1}{L_{tot}} \left[\int_{z=0}^{L_{TPh}} h_{TPh} dz + \int_{z=0}^{L_{SPh}} h_{SPh} dz \right] \tag{24}$$

Where $L_{tot} = L_{TPh} + L_{SPh}$

$$h_{TPh} = \frac{Nu_{TPh} k_l}{D} \tag{25}$$

$$h_{SPh} = \frac{Nu_{SPh} k_g}{D} \tag{26}$$

4. NUMERCAL ANALYSIS OF THE HEAT SPREADER

The computational fluid dynamics software package Fluent 6.0 and Gambit 2.0 were used to conduct a numerical analysis of the heat spreader. The 3D double precision option was used with the SIMPLE algorithm to solve the continuity equation. The QUICK algorithm was used as the converging criteria for both the momentum and energy equations. The Gambit 2.0 software was used to generate the mesh and Fluent was used to solve the problem numerically. The surface area of the heat spreader is 50.8×50.8 mm^2. The size of the CPU heat source was 19.05×19.05 mm^2. The CPU was located at the bottom-center of the heat spreader. To simplify the analysis, the contact resistance between the heat spreader and the CPU was neglected. In addition, any heat losses from the sides

and bottom of the heat spreader and CPU were neglected. The heat from the top surface of the CPU dissipates to the cold plate evaporator via the heat spreader. Six steady state cases were run with different heat spreader thickness of 2.5, 5.0, 7.5, 10.0, 12.5, and 15.0 mm. For each thickness, CPU heat fluxes of 55, 62, and 69 W/cm^2 were analyzed.
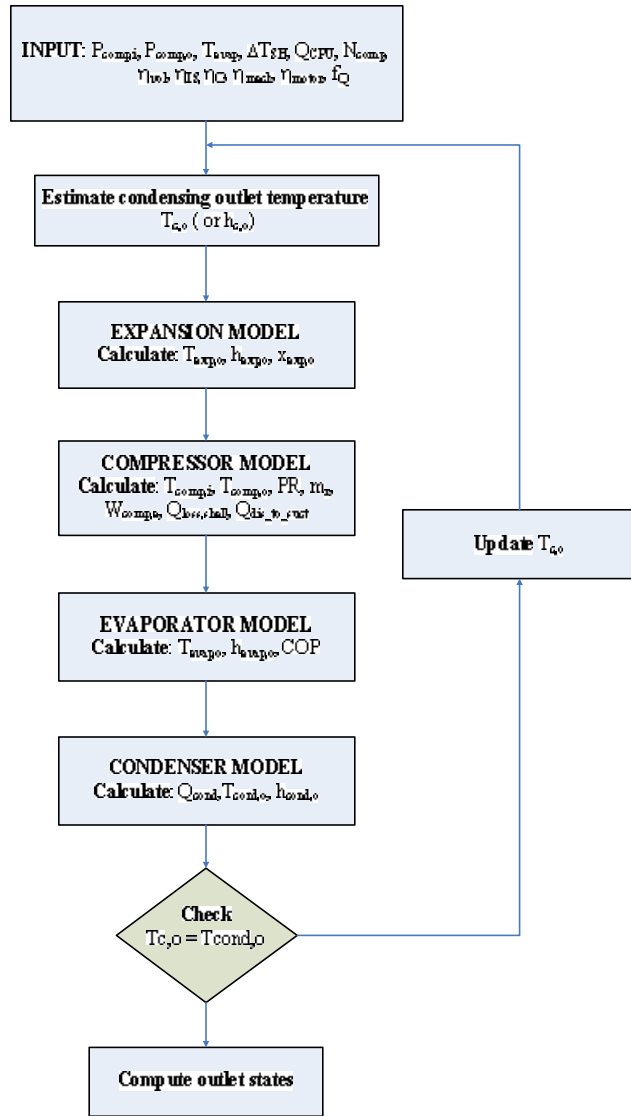
Figure 3: Refrigeration system model.
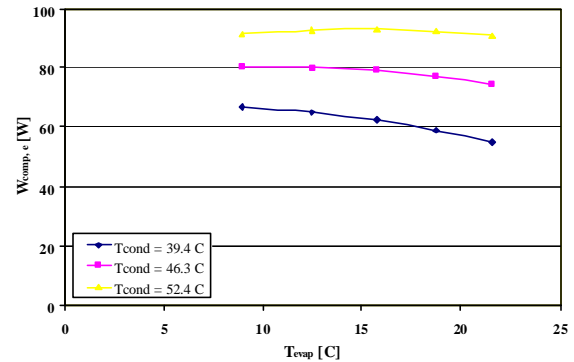
Figure 4: Compressor power input versus evaporating and condensing temperatures.
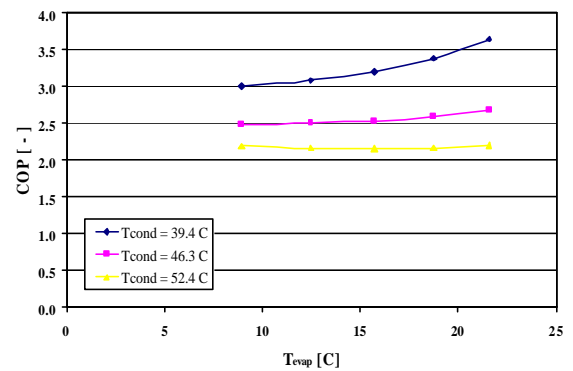
Figure 5: COP versus evaporating and condensing temperatures.
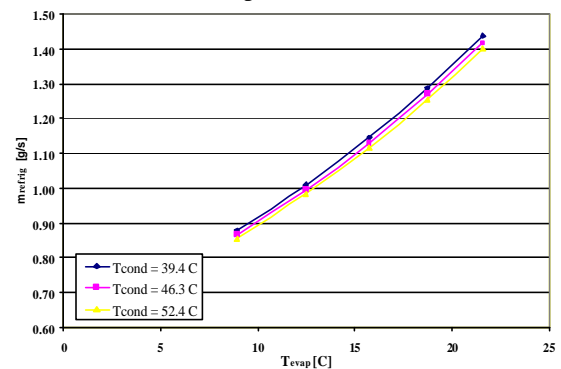
Figure 6: Refrigerant mass flow rate versus evaporating and condensing temperature.

5. NUMERCAL RESULTS

5.1 System Simulation Model Validation

The results of the system simulation model were compared to the experimental data as depicted in Table 1. The model predicts the measured system performance reasonable well. However, there is a significant error in the

prediction of the heat rejection rate of the condenser due to the use of the lump capacitance model in the condenser. In addition, the experimental bread board system experienced significant heat loss from the connecting piping.

Table 1: Comparison of experimental results and modeling results

Test	$T_{comp,i}$ [°C]	$P_{comp,i}$ [kPa]	$P_{comp,o}$ [kPa]	Q_{evap} [W]	h_r [W/m²-K]	T_{evap} [°C]		Error [%]	DT_{sup} [°C]		Error [%]	T_{cond} [°C]		Error [%]
	Input of Refrigeration Model				Model	Exp	Model		Exp	Model		Exp	Model	
1	15.13	454	1094	185.8	7164.33	12.72	12.75	-0.24	2.41	2.38	1.12	40.42	42.76	-5.79
2	18.69	507.6	1141	211.2	7311.50	16.18	16.21	-0.19	2.51	2.48	1.16	41.54	44.37	-6.81
3	19.98	532.3	1244	195.9	6164.13	17.69	17.71	-0.11	2.29	2.27	0.92	45.47	47.72	-4.95
4	19.02	497.9	1094	219.1	7627.12	15.58	15.60	-0.13	3.43	3.42	0.41	39.66	42.76	-7.82
5	13.67	426.9	1120	162.4	6500.28	10.86	10.88	-0.18	2.82	2.79	0.92	42.10	43.66	-3.71
6	16.42	465.2	1233	172	6285.69	13.48	13.50	-0.15	2.95	2.92	0.88	45.85	47.37	-3.32
7	17.18	485.1	1247	173.5	5976.45	14.77	14.79	-0.14	2.41	2.39	0.62	46.11	47.82	-3.71
8	19.93	508.9	1153	219.6	7628.32	16.27	16.29	-0.12	3.67	3.64	0.68	41.85	44.77	-6.98
9	17.24	483.4	1135	199	7225.53	14.66	14.68	-0.14	2.58	2.56	0.58	41.67	44.17	-6.00

Test	$T_{comp,o}$ [°C]		Error [%]	m_{refrig} [g/s]		Error [%]	Q_{cond} [W]		Error [%]	$W_{comp,e}$ [W]		Error [%]	COP_{system} [-]		Error [%]
	Exp	Model		Exp	Model		Exp	Model		Exp	Model		Exp	Model	
1	43.99	42.76	2.80	1.125	1.049	6.80	191.1	232.0	-21.41	74.50	72.20	3.08	2.494	2.573	-3.17
2	45.43	44.37	2.33	1.290	1.175	8.88	214.8	258.6	-20.40	77.81	74.08	4.80	2.715	2.851	-5.01
3	48.82	47.72	2.25	1.261	1.230	2.50	202.7	248.0	-22.32	88.43	81.32	8.04	2.215	2.409	-8.76
4	44.66	42.76	4.25	1.306	1.150	11.98	223.8	264.3	-18.11	73.70	70.66	4.12	2.972	3.101	-4.34
5	45.65	43.66	4.36	1.005	0.979	2.63	169.3	210.2	-24.15	75.59	74.67	1.22	2.148	2.175	-1.26
6	48.39	47.37	2.11	1.115	1.063	4.68	178.6	224.5	-25.70	84.79	82.04	3.25	2.029	2.096	-3.30
7	48.71	47.82	1.83	1.133	1.113	1.76	180.9	226.4	-25.17	86.40	82.72	4.26	2.008	2.097	-4.43
8	46.19	44.77	3.07	1.329	1.171	11.93	222.4	267.6	-20.33	77.99	75.02	3.81	2.816	2.930	-4.05
9	45.38	44.17	2.67	1.222	1.116	8.67	204.00	246.7	-20.91	77.06	72.47	5.96	2.583	2.670	-3.37

5.2 System Performance

The system performance was predicted using the system simulation model for evaporating temperature ranging from 10 to 20 °C and condensing temperature ranging from 40 to 60 °C. Figure 4 shows the compressor power input as a function of the evaporating and condensing temperatures. For a fixed condensing temperature, the compressor power input decreases as the evaporating temperature increases due to the decrease of the pressure ratio. For a fixed evaporating temperature, the compressor power input increases as the condensing temperature increases due to the increase of the pressure ratio. The COP and refrigerant mass flow rates as a function of the evaporating and condensing temperatures are depicted in Figure 5 and Figure 6, respectively. For a fixed cooling capacity of 200 W, the COP increases with increasing evaporating temperature or decreasing condensing temperature. For a fixed condensing temperature, the mass flow rate increases as the evaporating temperature increases. For a fixed evaporating temperature, the mass flow rate decreases as the condensing temperature increases. The numerical values of the system simulation results are shown in Table 2.

Table 2: System performance predictions by the system model

Test	$T_{comp,i}$ [°C]	$P_{comp,i}$ [kPa]	$P_{comp,o}$ [kPa]	Q_{evap} [W]	h_r [W/m²-K]	T_{evap} [°C]	DT_{sup} [°C]	T_{cond} [°C]	m_{refrig} [g/s]	Q_{cond} [W]	$W_{comp,elec}$ [W]	COP_{system} [-]
1	22.0	400	1000	200	7550.97	8.93	13.07	39.39	0.878	242.7	66.70	2.999
2	22.0	450	1000	200	7691.24	12.47	9.52	39.39	1.009	241.6	65.05	3.075
3	22.0	500	1000	200	6692.33	15.73	6.27	39.39	1.146	240.0	62.46	3.202
4	22.0	550	1000	200	5781.93	18.75	3.25	39.39	1.288	237.8	59.04	3.387
5	22.0	600	1000	200	5086.73	21.57	0.43	39.39	1.436	235.1	54.87	3.645
6	22.0	400	1200	200	7521.54	8.93	13.07	46.31	0.866	251.2	80.22	2.493
7	22.0	450	1200	200	7660.67	12.47	9.52	46.31	0.996	251.3	80.10	2.497
8	22.0	500	1200	200	6917.94	15.73	6.27	46.31	1.130	250.6	79.05	2.530
9	22.0	550	1200	200	5974.71	18.75	3.25	46.31	1.270	249.4	77.15	2.592
10	22.0	600	1200	200	5250.93	21.57	0.43	46.31	1.416	247.7	74.50	2.685
11	22.0	400	1400	200	7496.44	8.93	13.07	52.42	0.856	258.7	91.69	2.181
12	22.0	450	1400	200	7634.97	12.48	9.52	52.42	0.984	259.4	92.87	2.154
13	22.0	500	1400	200	7132.26	15.73	6.27	52.42	1.117	259.6	93.09	2.148
14	22.0	550	1400	200	6157.50	18.75	3.25	52.42	1.255	259.2	92.47	2.163
15	22.0	600	1400	200	5407.75	21.57	0.43	52.42	1.399	258.3	91.08	2.196

5.3 Heat Spreader Design Analysis

The temperature profiles of the heat spreader for a heat dissipation of 55 W/cm^2 and an average R-134a heat transfer coefficient of 7164.33 W/m^2-K for a variety of heat spreader thickness are depicted in Figure 7. Figure 8 presents the temperature profile at the vertical-center of the heat spreader for a thickness of 7.5 mm and a heat dissipation of 55 W/cm^2 at two locations, i.e., at the top surface of the CPU and at the top surface of the heat spreader. The temperature profile of the heat spreader with a thickness of 7.5 mm for various heat dissipations is shown in Figure 9. It can be seen from Figure 7 (c) and Figure 9 (a) to (b) that the maximum temperature increases as the heat dissipation increases from 55 to 62, and then to 69 W/cm^2 for the same heat spreader thickness of 7.5 mm, due to the additional heat flux.

The minimum and maximum temperatures of the heat spreader for a heat dissipation of 55 W/cm^2 as a function of different heat spreader thicknesses and average refrigerant heat transfer coefficients are presented in Table 3. The heat spreader thickness of 7.5 mm is the optimum thickness, since there is a more uniform temperature across the thickness of the heat spreader.
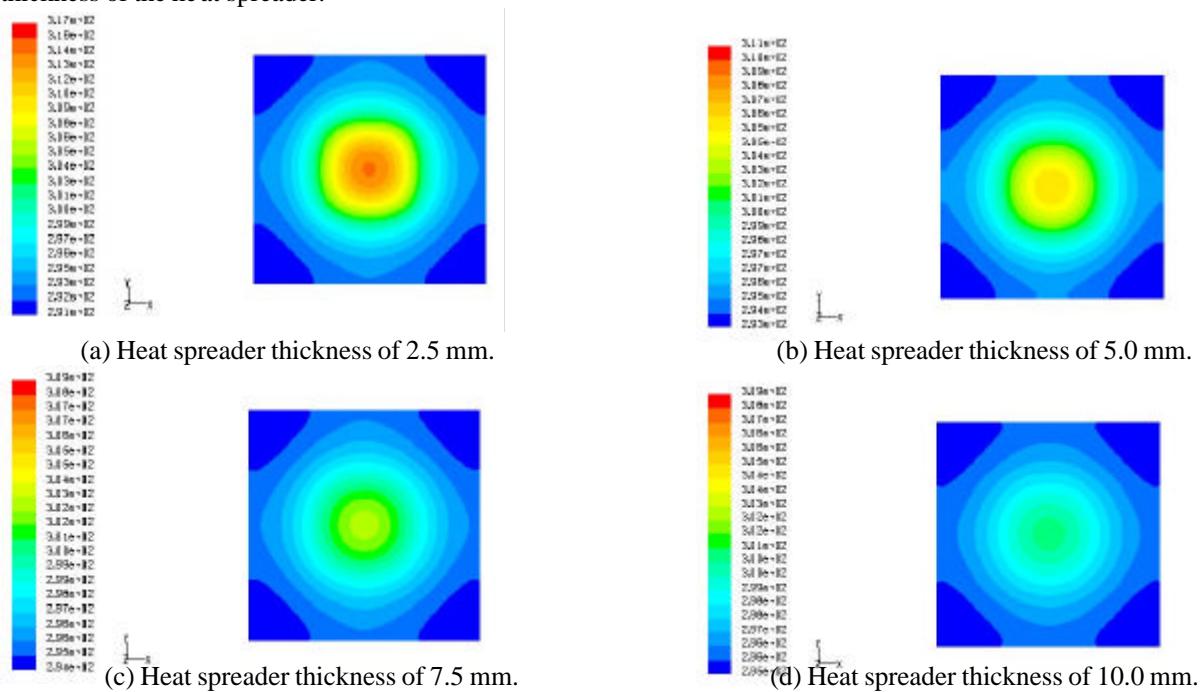

(a) Heat spreader thickness of 2.5 mm.

(b) Heat spreader thickness of 5.0 mm.

(c) Heat spreader thickness of 7.5 mm.

(d) Heat spreader thickness of 10.0 mm.

Figure 7: Temperature profile of the heat spreader for heat dissipation of 55 W/cm^2 and average heat transfer coefficient of R-134a of 7164.33 W/m^2-K.

(a) Top surface of CPU.

(b) Top surface of heat spreader.
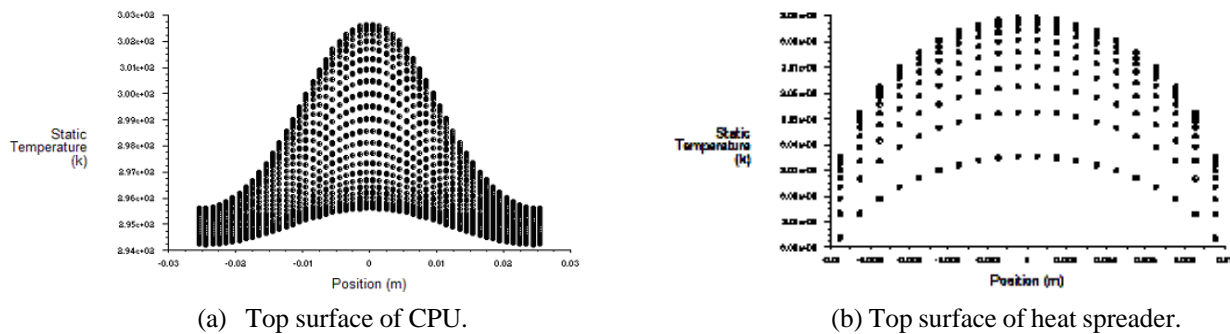
Figure 8: Temperature profile at the centerline of the heat spreader for a thickness of 7.5 mm and a heat dissipation of 55 W/cm^2.

(a) Heat dissipation of 62 W/cm^2.

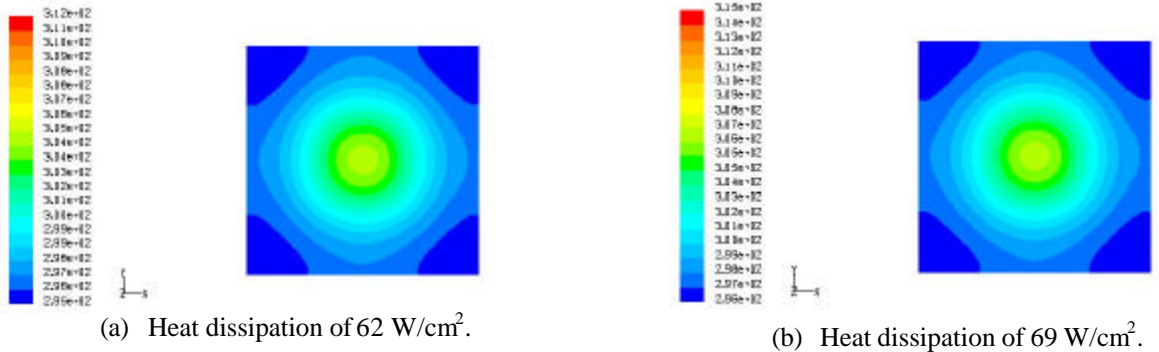(b) Heat dissipation of 69 W/cm^2.

Figure 9: Temperature profile of heat spreader with thickness of 7.5 mm for various heat dissipations.

Table 3: Temperature range at top surface of heat spreader for various conditions.

Thickness [mm]	Average R-134a heat transfer coefficient [W/m^2-K]	Minimum temperature [K]	Maximum temperature [K]	Thickness [mm]	Average R-134a heat transfer coefficient [W/m^2-K]	Minimum temperature [K]	Maximum temperature [K]
2.5	2000.0	316	349	10.0	2000.0	323	337
	3000.0	304	335		3000.0	310	337
	4000.0	298	328		4000.0	303	317
	5000.0	295	323		5000.0	299	313
	6000.0	292	320		6000.0	297	311
	7164.3	291	317		7164.3	295	309
5.0	2000.0	320	340	12.5	2000.0	323	337
	3000.0	307	327		3000.0	310	324
	4000.0	301	320		4000.0	304	317
	5000.0	297	316		5000.0	300	313
	6000.0	295	313		6000.0	297	311
	7164.3	293	311		7164.3	295	309
7.5	2000.0	322	337	15.0	2000.0	337	351
	3000.0	309	324		3000.0	325	338
	4000.0	303	318		4000.0	318	332
	5000.0	299	314		5000.0	314	328
	6000.0	296	311		6000.0	312	325
	7164.3	294	309		7164.3	310	323

6. CONCLUSIONS

A numerical simulation of a miniature-scale vapor compression refrigeration system was developed to predict its system performance for electronics cooling. In addition, the Fluent software was employed to simulate the temperature profile in the heat spreader connecting the heat source CPU to the cold plate evaporator. The results of the system simulation model show reasonable agreement with nine experimental test results taken with a bread board system. The model will be used in future studies to improve the design of the experimental setup. In addition, the analysis of the heat spreader indicated that an optimum thickness of the heat spreader can be found for the given operating conditions.

NOMENCLATURE

Bo	Boiling number	(-)	Fr	Froude number	(-)
Co	Convection number	(-)	f_Q	Heat loss coefficient of compressor	(-)
D	Diameter	(m)	G	Mass flux	(kg/s-m^2)
F_{fl}	Fluid-surface parameter	(-)	h	Enthalpy	(J/kg-K)

L	Length	(m)	dis	Discharge	
$\dot{m}$	Refrigerant mass flow rate	(kg/s)	e	Electricity	
N	Compressor speed	(RPM)	evap	Evaporator	
Nu	Nusselt number	(-)	exp	Expansion	
Pr	Prandtl number	(-)	f	Fluid or liquid or friction factor	
$\dot{Q}$	Heat loss or heat transfer rate	(W)	g	Gas or vapor	
q''	Heat flux	(W/m^2)	i, in	Inlet	
Re	Reynolds number	(-)	isen	Isentropic	
$\dot{W}$	Power consumption or power input	(W)	lo	Liquid only	
x	Quality	(-)	mech	Mechanical	

Greek symbol

h	Efficiency	(%)	motor	Motor	
r	Density	(kg/m^3)	NBD	Nucleate boiling dominant	
			o	Overall	

Subscript

CBD	Convective boiling dominant		refrig	Refrigerant	
comp	Compressor		SPh	Single phase	
cond	Condenser		suct	Suction	
			TPh	Two-phase	
			vol	Volumetric	

REFERENCES

[1] Phelan, P.E., 2001, Current and Future Miniature Refrigeration Cooling Technologies for High Power Microelectronics, Semiconductor Thermal Measurement and Management Symposium: Seventeenth Annual IEEE, San Jose, CA USA, March 20-22, 2001, pp. 158-167.

[2] Kandlikar, S.G., 1999, Flow Boiling Heat Transfer Coefficient in Microchannels-Correlation and Trends, http://www.rit.edu/~taleme/78_IHTC02_1178.pdf.

[3] Incropera, F.P. and Dewitt, D.P., 2002, Fundamentals of Heat and Mass Transfer, 5th edition, John Wiley &Sons, Inc.

[4] Braun, E.J., 2001, Lecture notes of ME 518: Analysis of Energy Utilization Systems, Evaporator and Condenser analysis.

[5] Mudawar, I., 2002, Lecture notes of ME 506: Two-phase Flow and Heat Transfer, Homogeneous two-phase flow model.

ACKNOWLEDGEMENT